

# Novel Mesoporous Carbon-Carbonaceous Materials Nanostructures Decorated with MnO<sub>2</sub> Nanosheets for Supercapacitors

Zhong Quan Wen<sup>1,\*</sup>, Min Li<sup>1</sup>, Shi Jin Zhu<sup>2</sup>, Tian Wang<sup>2</sup>

<sup>1</sup>College of Optoelectronic Engineering, Key Laboratory of Fundamental Science of Micro/Nano-Devices and System Technology, Chongqing University, Chongqing 400044, PR China

<sup>2</sup>College of Materials Science and Engineering, Chongqing University, Chongqing 400044, PR China

\*E-mail: [wenzq66@163.com](mailto:wenzq66@163.com)

Received: 30 November 2015 / Accepted: 17 December 2015 / Published: 1 February 2016

---

Herein, we fabricated a range of flexible nanocomposite electrodes by combining mesoporous carbon (MC) with graphene nanosheets (GNS), carbon nanotubes (CNT) and carbon spheres (CS) respectively, followed by the decoration of MnO<sub>2</sub> nanosheets using a developed etching method approach. Results after a series of electrochemical measurements demonstrated that as-synthesized nanostructures realized the larger specific capacitance of 326 F g<sup>-1</sup> and an increase specific capacitance was found after 1000 cycles interestingly. Indeed, these findings will capacitate low-cost nanocomposite carbon materials fascinating for long cycling and electrochemically stable supercapacitors.

---

**Keywords:** mesoporous carbon; graphene nanosheets; carbon nanotubes; carbon spheres; MnO<sub>2</sub>; supercapacitors

## 1. INTRODUCTION

Supercapacitors, as ideal energy storage and conversion devices, have captured intense attention mostly because of their outstanding electrochemical performance such as long cycle life, high power density, shorter charge duration and low environmental impact [1-5]. According to charge storage mechanisms, supercapacitors are generally categorized as electrochemical double layer capacitors (EDLCs) and pseudocapacitors because their energy storage and conversion processes occur in two different ways [6-8]. EDLCs store energy electrostatically on the basis of charge separation at

the electrode/electrolyte interfaces, and pseudocapacitors utilize reversible and rapid superficial Faradaic reactions happening at the electrode [9].

Recently, carbon-active materials (e.g., CNT, graphene) have been extensively applied to supercapacitor electrodes as they possess favorable properties of pleasurable electrical conductivity, versatile size dimensionality and strong structural integrity [10-12]. However, carbon-based electrodes suffer from dreadful specific capacitance. Accordingly, transition metal oxides (e.g.,  $\text{MnO}_2$ ,  $\text{Co}_3\text{O}_4$ ,  $\text{NiO}$ ) have been incorporated into the electrodes for supercapacitors owe to the large specific capacitance originating from stable redox reactions [13-15]. Particularly, as a pseudocapacitive electrode material,  $\text{MnO}_2$  manifests outstanding merits on account of its high electrochemical activity, environmental friendliness, high natural abundance and low cost. Unfortunately, due to its unfavorable electrical conductivity and electrochemical dissolution during cycling,  $\text{MnO}_2$  can not generally realize the theoretical specific capacitance of  $\sim 1370 \text{ F g}^{-1}$  [16-18]. As a matter of fact, by combining  $\text{MnO}_2$  with carbonaceous materials [4,12,19] the electrochemical capacitance can be substantially enhanced and the supercapacitance performance can be significantly improved when these composites are designed as 3-dimensional (3D) composites with increased surface area.

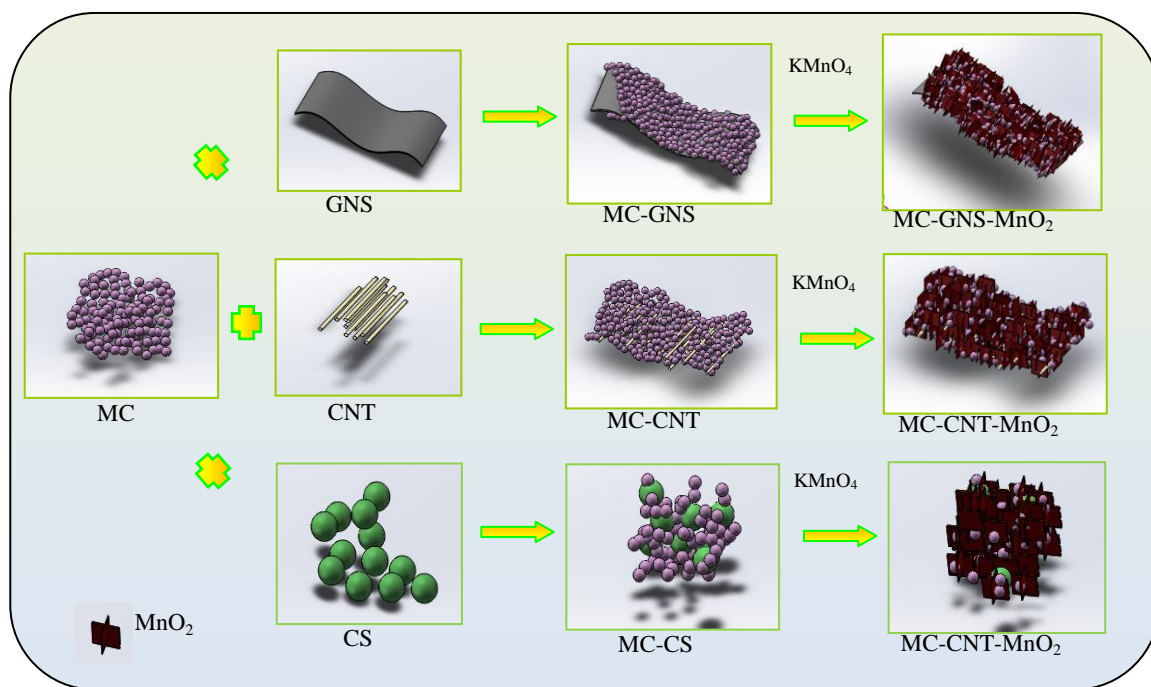


**Figure 1.** Sketch map presenting the synthetic process of the as-prepared samples in this work.

Herein, a cost-effective and flexible method has been established to manufacture 3-dimensional (3D) MC-GNS, MC-CNT and MC-CS composites, which are utilized as skeletons to support the  $\text{MnO}_2$ . Schematic diagram displaying our concept and preparation process is presented in Fig. 1. The idea here is to use unique mesoporous carbon and carbonaceous materials (GNS, CNT and CS) nanocomposite structures and combine them with  $\text{MnO}_2$  nanosheets to build for the first time unique 3D composites we propose should have advanced supercapacitor performances. Utilizing simple

hydrothermal method, MC-GNS-MnO<sub>2</sub>, MC-CNT-MnO<sub>2</sub> and MC-CS-MnO<sub>2</sub> nanostructures are successfully synthesized for the first time, exhibiting higher specific capacitance and stable cycling performance.

## 2. EXPERIMENTAL SECTION

### 2.1 Preparation of MC-GNS, MC-CNT and MC-CS nanocomposites

According to a modified hydrothermal method used in an earlier report [20], MC-GNS, MC-CNT and MC-CS were synthesized here. Typically, 12 g of glucose and 30 mg of graphene nanosheets (GNS) were dissolved in distilled water (35 mL), followed by the addition of ethylenediamine (EDA) (2 mL). The mixture was poured into a 50-mL Teflon-lined stainless steel autoclave, maintaining at 180 °C for 4 h. And the solid precipitates were gathered by several rinse-centrifugation cycles when the temperature drops to the environment, thus obtaining MC-GNS after being rinsed with ethanol and distilled water. Similarly, 30 mg of carbon nanotubes (CNT) and carbon spheres (CS) instead of graphene nanosheets and obtained MC-CNT and MC-CS, respectively.

### 2.2 Synthesis of MC-GNS-MnO<sub>2</sub>, MC-CNT-MnO<sub>2</sub> and MC-CS-MnO<sub>2</sub>

The MC-GNS-MnO<sub>2</sub>, MC-CNT-MnO<sub>2</sub> and MC-CS-MnO<sub>2</sub> nanocomposites were synthesized by a developed etching method [22]. Quintessentially, MC-GNS powders (10 mg) were dispersed into 20 mL of distilled water. After ultrasonication for 10 minutes, KMnO<sub>4</sub> solution (5 mL) and H<sub>2</sub>SO<sub>4</sub> solution (0.8 mL, 50 mM) were added in sequence. The mixed liquor was washed, centrifuged and dried at 60 °C after stirring for 2 h. Thus the solid precipitates obtained are named as MC-GNS-MnO<sub>2</sub>-10, MC-GNS-MnO<sub>2</sub>-20, and MC-GNS-MnO<sub>2</sub>-50, representing the different KMnO<sub>4</sub> concentrations of 10, 20, and 50 mM, respectively. Furthermore, MC-CNT-MnO<sub>2</sub>-10, MC-CNT-MnO<sub>2</sub>-20, MC-CNT-MnO<sub>2</sub>-50, MC-CS-MnO<sub>2</sub>-10, MC-CS-MnO<sub>2</sub>-20 and MC-CS-MnO<sub>2</sub>-50 were synthesized in the same way.

### 2.3. Characterization

The chemical compositions and crystal structures of as-synthesized products were recorded on powder X-ray diffraction (XRD, D/max 1200, Cu K $\alpha$ ), and thermogravimetric analyzer-differential scanning calorimeter (TGA-DSC NETZSCH STA 449C). The structure and morphology of as-obtained nanocomposites were performed with a focused ion beam scanning electron microscopy (Zeiss Auriga FIB/SEM). We tested the specific surface area by N<sub>2</sub> adsorption/desorption isotherm at 77 K, and the pore size distributions were calculated from the adsorption curve with the Barrett-Joyner-Halenda (BJH) method.

### 2.4 Electrochemical measurements

All the electrochemical measurements of nanocomposites synthesized in this work were performed by the electrochemical workstation (CHI 660E) with the electrolyte of 1 M  $\text{Na}_2\text{SO}_4$  aqueous solution in a three-electrode electrochemical cell which universally composed of a saturated calomel electrode (SCE) and platinum plate respectively used as the reference electrode and the counter electrode. The working electrode was composed of 70wt% as-obtained active materials, 20wt% carbon black and 10wt% polyvinylidene fluoride (PVDF), which was pasted on the nickel foam as a current collector. Finally, the electrodes were then dried at 120 °C under vacuum overnight to remove the solvent and water.

Cyclic voltammetry (CV) in the voltage between 0 and 1.0 V were carried out to measure the capacitive behaviors of the as-obtained nanocomposites. Galvanostatic charge-discharge tests were performed at varied current densities in the same potential range as the CV experiments. EIS measurements were performed at open circuit voltage in a frequency range from 0.01 Hz to 100 kHz, applying an AC voltage with 5 mV amplitude. The charge-discharge cycling was performed by 1000 cycles at a current density of 2 A  $\text{g}^{-1}$ .

## 3. RESULTS AND DISCUSSION

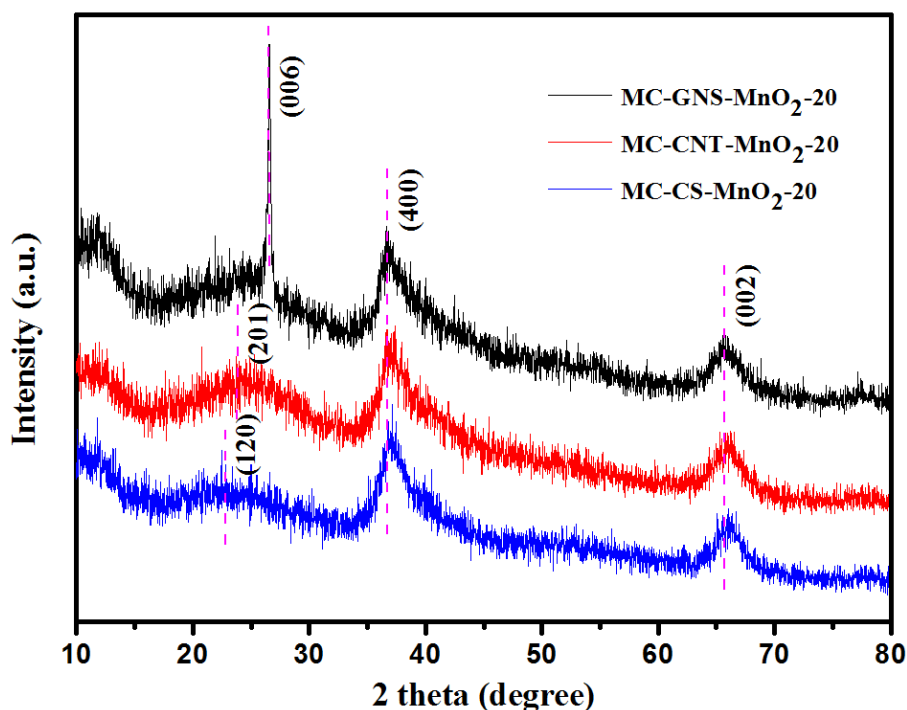


**Figure 2.** XRD patterns of MC-GNS-MnO<sub>2</sub>-20, MC-CNT-MnO<sub>2</sub>-20 and MC-CS-MnO<sub>2</sub>-20.

Fig. 2 illustrates the XRD patterns of as-obtained nanocomposites, which reveals that the diffraction peaks at  $2\theta=37.0^\circ$  and  $65.8^\circ$ , assigning to the (400) and (002) crystal planes of MnO<sub>2</sub>

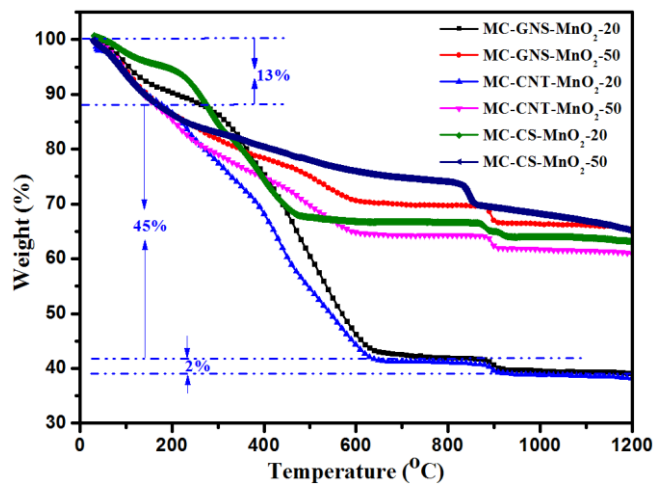


**Figure 3.** TGA curves of MC-GNS-MnO<sub>2</sub>-20, MC-GNS-MnO<sub>2</sub>-50, MC-CNT-MnO<sub>2</sub>-20 and MC-CNT-MnO<sub>2</sub>-50.

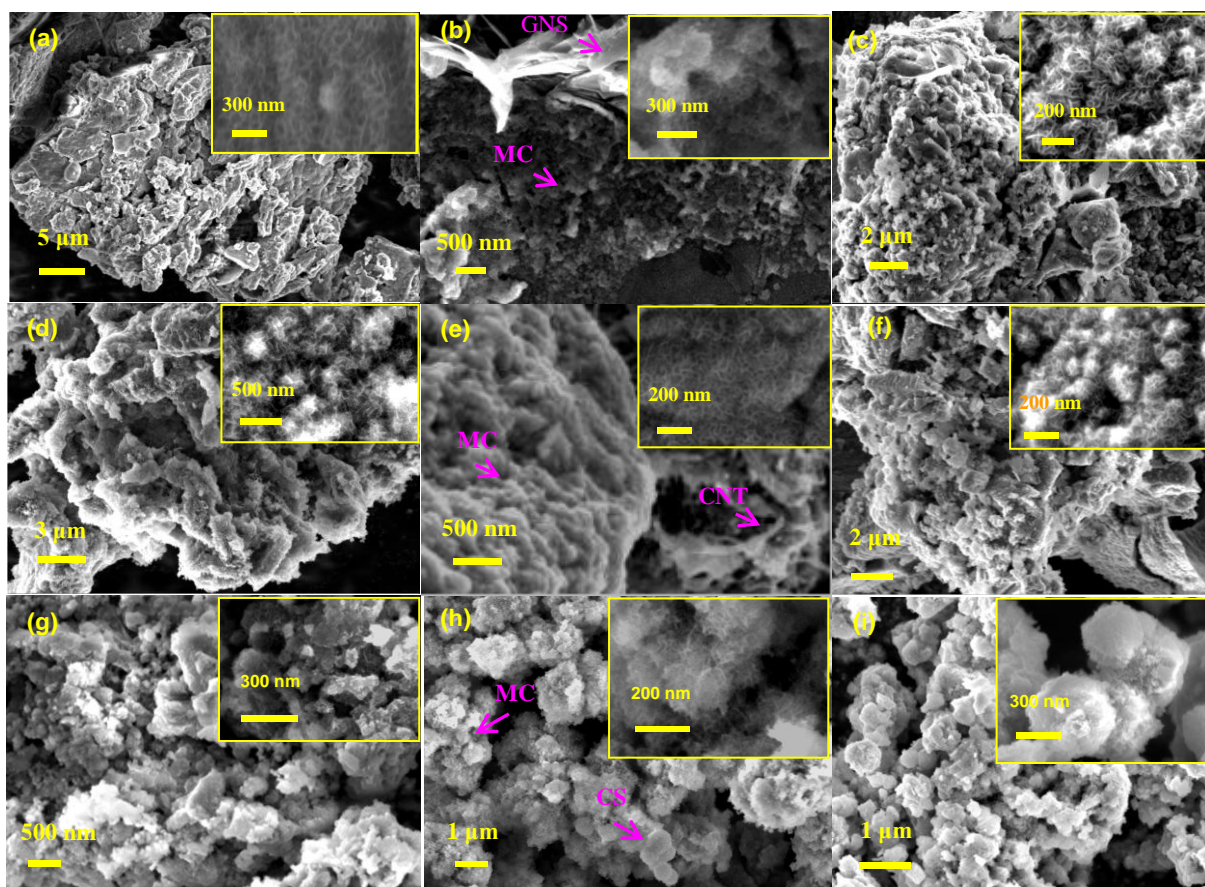


**Figure 4.** SEM graphs of MC-GNS-MnO<sub>2</sub>-10 (a), MC-GNS-MnO<sub>2</sub>-20 (b), MC-GNS-MnO<sub>2</sub>-50 (c), MC-CNT-MnO<sub>2</sub>-10 (d), MC-CNT-MnO<sub>2</sub>-20 (e), MC-CNT-MnO<sub>2</sub>-50 (f), MC-CS-MnO<sub>2</sub>-10 (j), MC-CS-MnO<sub>2</sub>-20 (h) and MC-CS-MnO<sub>2</sub>-50 (i).

(JCPDS no. 44-0141) [21] and an expanding peak of the mesoporous carbon around 25°, demonstrating its amorphous nature. Carefully investigating, we can discover that it is different

between three curves at 25°. The main reason may be the difference of carbon materials doped in the MC.

In order to estimate the content of MnO<sub>2</sub> in the nanocomposites, the as-obtained samples are researched utilizing TGA (Fig. 3). On the basis of the results, 39.1%, 65.5%, 38.2%, 61%, 63.2% and 65.1% of MnO<sub>2</sub> contents are counted for the MC-GNS-MnO<sub>2</sub>-20, MC-GNS-MnO<sub>2</sub>-50, MC-CNT-MnO<sub>2</sub>-20, MC-CNT-MnO<sub>2</sub>-50, MC-CS-MnO<sub>2</sub>-20 and MC-CS-MnO<sub>2</sub>-50, respectively, signifying that the content of MnO<sub>2</sub> could be controlled by changing the concentrations of KMnO<sub>4</sub> solution. What is the most important is that the TGA results will be beneficial to us to calculate the specific capacitance of the samples precisely.

Scanning electron microscopy (SEM) is utilized to investigate morphologies of the as-synthesized samples, and the images are depicted in Fig. 4. From Fig. 4a, b and c we can see that MnO<sub>2</sub> nanosheets uniformly decorated on the MC-GNS nanostructures become thicker and denser apparently with increasing of the concentration of KMnO<sub>4</sub> solution. Notably, we can obviously observe the graphene nanosheets (GNS) doped in the mesoporous carbon (MC), consequently testifying the successful synthesis of the MC-GNS-MnO<sub>2</sub>. In addition, MC-CNT-MnO<sub>2</sub> with different content of MnO<sub>2</sub> is successfully prepared at the same moment (Fig. 4d, e and f). Consistent with the MC-GNS-MnO<sub>2</sub>, MC-CNT nanostructures are coated with the thicker and denser MnO<sub>2</sub> nanosheets as the concentration of KMnO<sub>4</sub> solution grow. Fig. 4e clearly exhibits the CNT combined with MC, which are decorated with MnO<sub>2</sub> nanosheets as well. Last but not the least, the SEM images of the MC-CS-MnO<sub>2</sub> are illustrated in Fig. 4g, h and i. Interestingly, some furry carbon spheres coated with MnO<sub>2</sub> jump into our sight (Fig. 4h and i). It is worth noting that the MC doped with different carbon materials (GNS, CNT and CS) in this work can facilitate the ion diffusion and electron transportation, owing to the interconnected skeletons which create adequate space highly required for high-performance supercapacitor electrodes materials [22]. All above findings signify that the pore structure and morphology of MC-GNS-MnO<sub>2</sub>, MC-CNT-MnO<sub>2</sub> and MC-CS-MnO<sub>2</sub> nanostructures could be controlled by changing the amount of KMnO<sub>4</sub>.

To further analyze the pore structure of the quintessential composites, N<sub>2</sub> adsorption/desorption technique is used. Fig. 5 presents the N<sub>2</sub> adsorption-desorption isotherms and the Barrett-Joyner-Halenda (BJH) pore size distribution curves (insets) of MC-GNS-MnO<sub>2</sub>-20, MC-CNT-MnO<sub>2</sub>-20 and MC-CS-MnO<sub>2</sub>-20, respectively. It is obvious that the isotherm ought to be assigned to type IV concluding the pronounced hysteresis loops [23], revealing that all of the samples enjoy a quintessential mesoporous structure and the insets in Fig. 5 further confirm the porosity of the samples. From the results of N<sub>2</sub> adsorption/desorption, MC-CS-MnO<sub>2</sub>-20 shows the higher specific area of 55.6 m<sup>2</sup> g<sup>-1</sup>. It is generally acknowledged that moderate BET surface area and the porous structure of these nanostructures could provide enhanced number of channels for efficient electrons and ions transport, contributing to outstanding electrochemical performance [24]. As working electrodes in a three-electrode electrochemical cell, the MC-GNS-MnO<sub>2</sub>, MC-CNT-MnO<sub>2</sub> and MC-CS-MnO<sub>2</sub> nanostructures have been employed to estimate the electrochemical performance in supercapacitors respectively. As it can be seen in Fig. 6a, the CV curves at the scan rate of 50 mV s<sup>-1</sup> of the as-synthesized hybrids demonstrate almost symmetric rectangular shapes more or less without obvious redox peaks, manifesting pleasurable capacitive behavior with swift charge transmission.

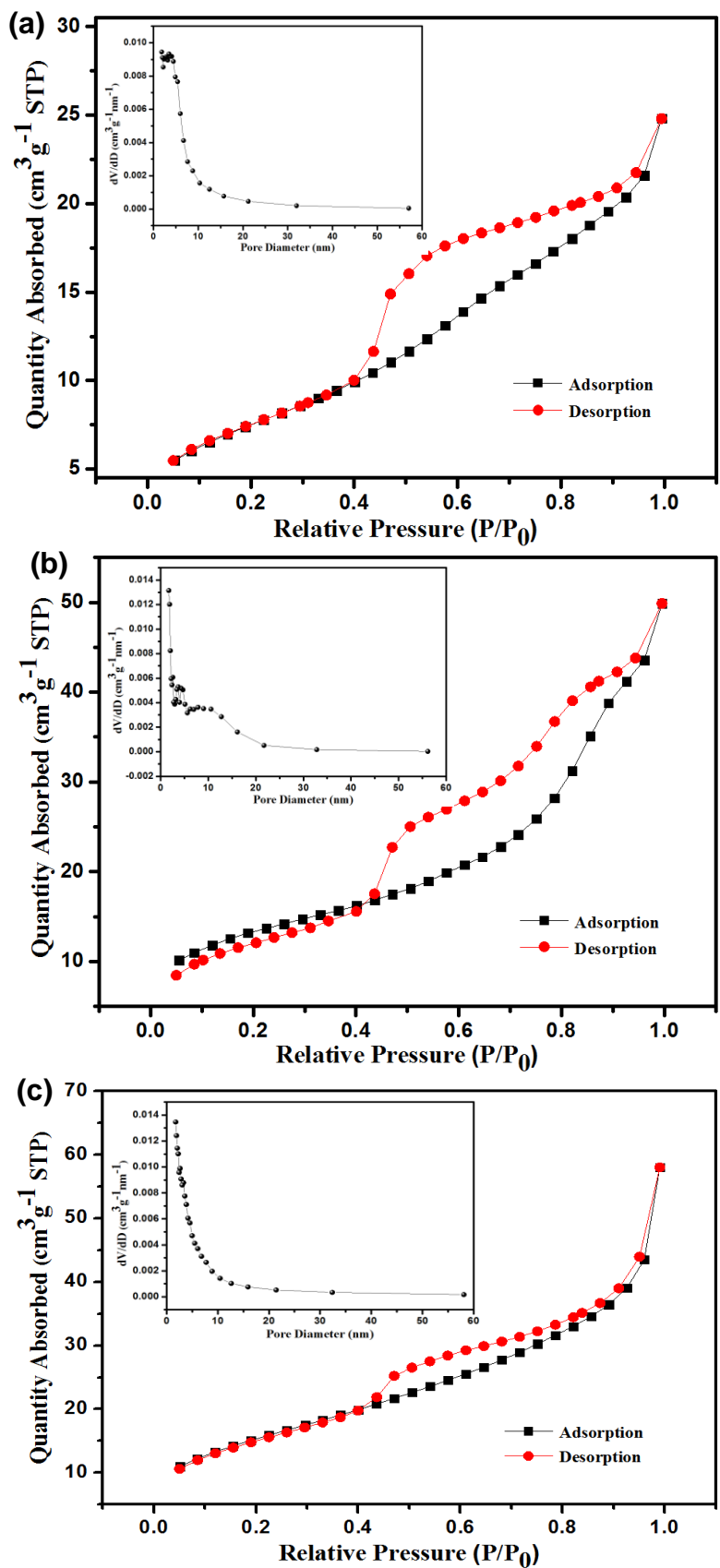


**Figure 5.** N<sub>2</sub> adsorption and desorption isotherms and their corresponding pore-size distribution curves (insets) of (a) MC-GNS-MnO<sub>2</sub>-20, (b) MC-CNT-MnO<sub>2</sub>-20, (c) MC-CS-MnO<sub>2</sub>-20.

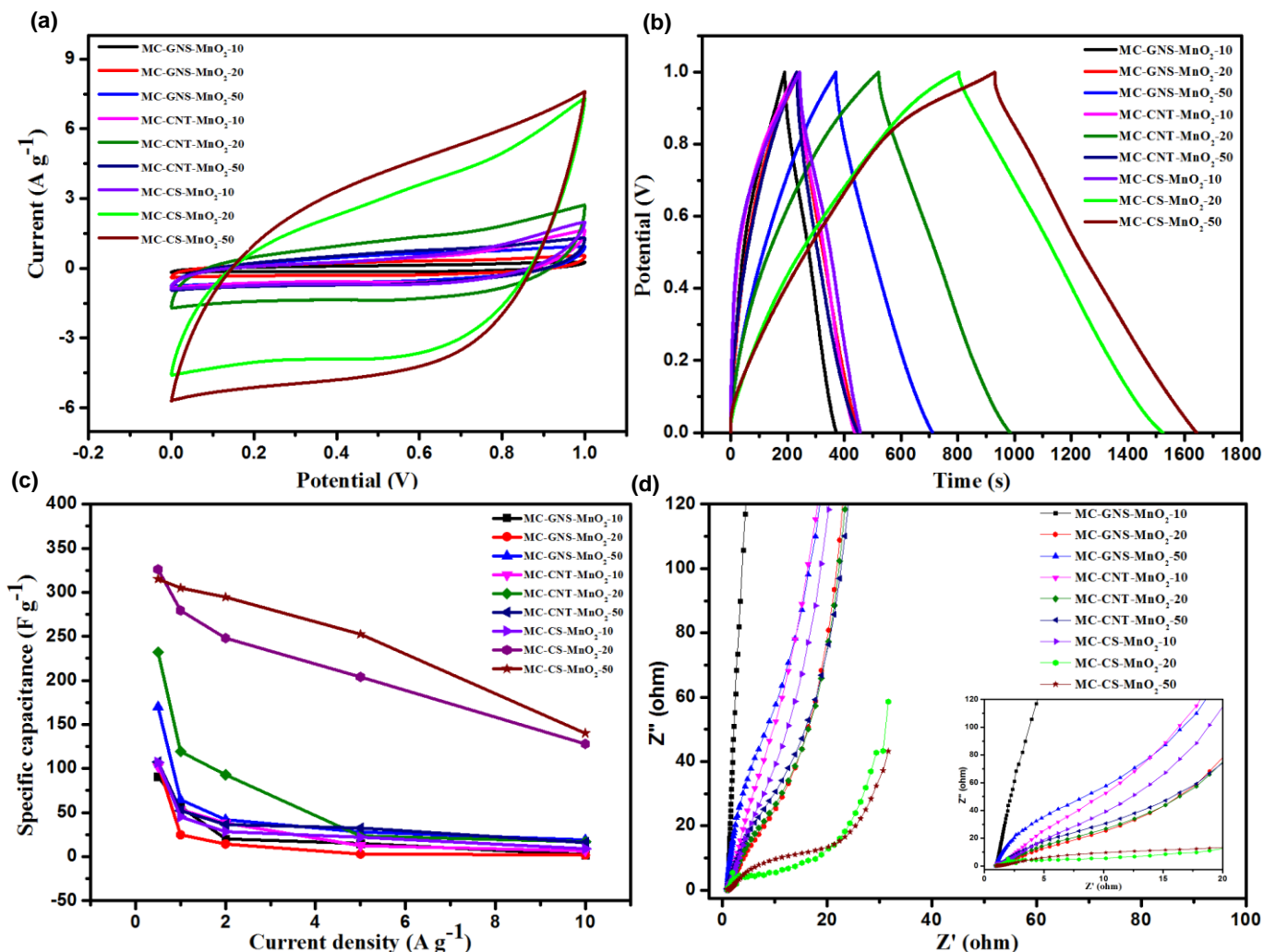


**Figure 6.** The electrochemical performance of the MC-GNS-MnO<sub>2</sub> and MC-CNT-MnO<sub>2</sub> nanomaterials electrodes measured in 1 M Na<sub>2</sub>SO<sub>4</sub> solution. (a) CV curves measured at a scan rate of 50 mV s<sup>-1</sup>. (b) Galvanostatic charge-discharge curves at the current density of 0.5 A g<sup>-1</sup>. (c) Specific capacitance at various current densities. (d) Electrochemical impedance spectrum in the frequency range from 0.01 Hz to 100 kHz at open circuit potential.

It is obvious that MC-CS-MnO<sub>2</sub>-20 and MC-CS-MnO<sub>2</sub>-50 enjoy the larger area with a slight deformation, signifying excellent capacitive and reversible behavior in the voltage between 0 and 1.0 V. It is noteworthy that MC-CNT-MnO<sub>2</sub>-20 possesses a larger area than that of MC-CNT-MnO<sub>2</sub>-50. The reason might be that MC-CNT-MnO<sub>2</sub>-50 nanostructures are coated with the denser MnO<sub>2</sub> nanosheets which impede effective transport of the electrolyte ions.

Figure. 6b presents the galvanostatic charge-discharge curves whose charging curves are nearly balanced to its homologous discharging counterpart, suggesting that the samples have super electrochemical performance and reversibility. Based on the equation [5,25,26]:  $C_s = (I\Delta t) / (m\Delta V)$ , where  $I$ ,  $\Delta t$ ,  $m$  and  $\Delta V$  are discharge current (A), the discharging time (s), the weight (g) of the electroactive materials (m), and the discharging potential range (V), respectively, the specific capacitances of the as-synthesized samples are calculated to be 105, 170, 232, 107.6, 326, 315 F g<sup>-1</sup> for

MC-GNS-MnO<sub>2</sub>-20, MC-GNS-MnO<sub>2</sub>-50, MC-CNT-MnO<sub>2</sub>-20, MC-CNT-MnO<sub>2</sub>-50, MC-CS-MnO<sub>2</sub>-20 and MC-CS-MnO<sub>2</sub>-50 at a current density of 0.5 A g<sup>-1</sup>, respectively, which can be also obtained in Fig. 6c displaying the specific capacitance of as-obtained samples at different current densities.

Electrochemical impedance spectroscopy (EIS) measurements of MC-GNS, MC-CNT and MC-CS decorated with MnO<sub>2</sub> nanosheets are performed in the frequency range from 0.01 to 100 kHz, as displayed in Fig. 6d. We can discover that the Nyquist plots are analogous in shape, consisted of the partial semicircle at high frequency and a linear component in the low frequency region. The semicircle at high frequency is associated with the charge-transfer resistance ( $R_{ct}$ ), and a nearly 90° of the vertical line at low frequency is observed, indicating an ideal capacitive behavior of electrochemical double-layer capacitor [27]. From the inset in Fig. 6d, the  $R_{ct}$  values are estimated to be about 3, 2.4, 2.8, 2.9, 2.6, 2.7, 3.4, 0.7 and 1.8 Ω for MC-GNS-MnO<sub>2</sub>-10, MC-GNS-MnO<sub>2</sub>-20, MC-GNS-MnO<sub>2</sub>-50, MC-CNT-MnO<sub>2</sub>-10, MC-CNT-MnO<sub>2</sub>-20, MC-CNT-MnO<sub>2</sub>-50, MC-CS-MnO<sub>2</sub>-10, MC-CS-MnO<sub>2</sub>-20 and MC-CS-MnO<sub>2</sub>-50, respectively.

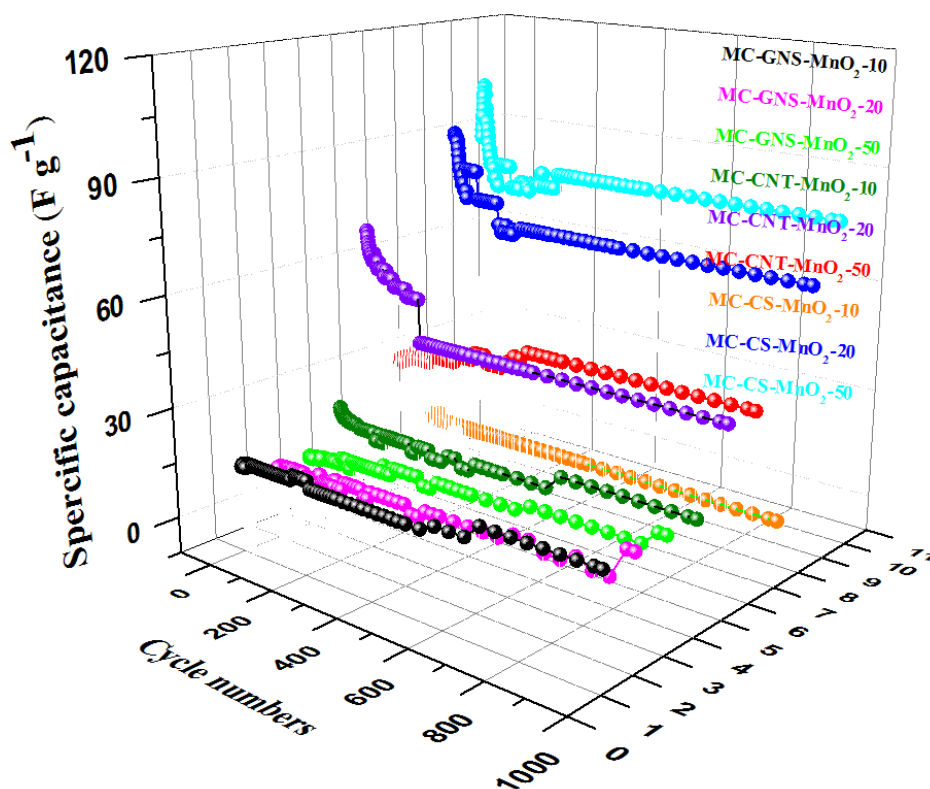


**Figure 7.** Variation of capacitance with cycle number at the current density of 2.0 A g<sup>-1</sup>.

It is universally acknowledged that electrochemical stability is one of the key properties that the supercapacitor devices need to have. Thus, as depicted in Fig. 7, the cycle stability is further investigated by repeating the CV measurements at the current density of 2 A g<sup>-1</sup> for 1000 cycles. After 1000 cycles, 147.06%, 227.27%, 217.39%, 98.04%, 58.82%, 138.89%, 88.89%, 73.66%, and 91.33% of the pristine capacitance is retained for MC-GNS-MnO<sub>2</sub>-10, MC-GNS-MnO<sub>2</sub>-20, MC-GNS-MnO<sub>2</sub>-50, MC-CNT-MnO<sub>2</sub>-10, MC-CNT-MnO<sub>2</sub>-20, MC-CNT-MnO<sub>2</sub>-50, MC-CS-MnO<sub>2</sub>-10, MC-CS-MnO<sub>2</sub>-20 and MC-CS-MnO<sub>2</sub>-50, respectively.

50, MC-CNT-MnO<sub>2</sub>-10, MC-CNT-MnO<sub>2</sub>-20, MC-CNT-MnO<sub>2</sub>-50, MC-CS-MnO<sub>2</sub>-10, MC-CS-MnO<sub>2</sub>-20 and MC-CS-MnO<sub>2</sub>-50, respectively, signifying super electrochemical stability as the supercapacitor electrode materials. To our surprise, augments on specific capacitance for the as-prepared nanocomposites are found after 1000 cycles, which is ascribed to the activation effect of electrochemical cycling.

#### 4. CONCLUSIONS

In summary, we have designed and prepared the nanocomposites combined mesoporous carbon (MC) with graphene nanosheets (GNS), carbon nanotubes (CNT) or carbon spheres (CS) and MnO<sub>2</sub>-nanostructures for the first time. Furthermore, the electrochemical performance of these nanostructures has been measured by CV, galvanostatic charge-discharge, EIS measurements and so on. It was found that MC-GNS-MnO<sub>2</sub>-20, MC-CS-MnO<sub>2</sub>-20 and MC-CS-MnO<sub>2</sub>-50 enjoyed the larger specific capacitance compared with other samples, and augments on specific capacitance for the as-prepared nanocomposites are found after 1000 cycles, presenting the more promising prospects in developing flexible, cost-effective and environment friendly supercapacitors.

#### ACKNOWLEDGEMENTS

The authors gratefully acknowledge the financial supports provided by National Natural Science Foundation of China (Grant no. 61474011).

#### References

1. Y. Y. Sun, W. H. Zhang, D. S. Li, L. Gao, C. L. Hou, Y. H. Zhang, Y. Q. Liu, *Electrochim. Acta*, 178 (2015) 823.
2. M. Huang, R. Mi, H. Liu, F. Li, X. L. Zhao, W. Zhang, S. X. He, Y. X. Zhang, *J. Power Sources*, 269 (2014) 760.
3. J. J. Chen, Y. Huang, X. Zhang, X. F. Chen, C. Li, *Ceram. Int.*, 41 (2015) 12680.
4. X. Y. Zhang, L. Q. Han, S. Sun, C. Y. Wang, M. M. Chen, *J. Alloy. Compd.*, 653 (2015) 539.
5. F. Li, Y. X. Zhang, M. Huang, Y. Xing, L. L. Zhang, *Electrochim. Acta*, 154 (2015) 329.
6. J. G. Wang, F. Y. Kang, B. Q. Wei, *Prog. Mater. Sci.*, 74 (2015) 51.
7. Y. X. Zhang, M. Huang, F. Li, X. L. Wang, Z. Q. Wen, *J. Power Sources*, 246 (2014) 449.
8. Y. L. Chen, L. H. Du, P. H. Yang, P. Sun, X. Yu, W. J. Mai, *J. Power Sources*, 287 (2015) 68.
9. M. Kuang, W. Zhang, X. L. Guo, L. Yu, Y. X. Zhang, *Ceram. Int.*, 40 (2014) 10005.
10. Y. J. Kang, H. Chung, M. S. Kim, W. Kim, *Appl. Surf. Sci.*, 355 (2015) 160.
11. M. Q. Sun, H. Li, J. Wang, G. C. Wang, *Carbon*, 94 (2015) 864.
12. S. J. Zhu, W. L. Cen, L. L. Hao, J. J. Ma, L. Yu, H. L. Zheng, Y. X. Zhang, *Mater. Lett.*, 135 (2014) 11.
13. J. Y. Zhou, H. Zhao, X. M. Mu, J. Y. Chen, P. Zhang, Y. L. Wang, Y. M. He, Z. X. Zhang, X. J. Pan, E. Q. Xie, *Nanoscale*, 7 (2015) 14697.
14. Y. X. Zhang, S. J. Zhu, X. D. Hao, C. P. Liu, Z. Q. Wen, *Ceram. Int.*, 40 (2014) 13381.
15. M. Huang, F. Li, X. L. Zhao, D. Luo, X. Q. You, Y. X. Zhang, G. Li, *Electrochim. Acta*, 152 (2015) 172.

16. J. X. Deng, X. Wang, X. J. Duan, P. Liu, *ACS Sustain Chem Eng.*, 3 (2015) 1330.
17. M. Huang, Y. X. Zhang, F. Li, L. L. Zhang, R.S. Ruoff, Z. Y. Wen, Q. Liu, *Sci. Rep.*, 4 (2014) 3878.
18. X. M. Feng, Z. Z. Yan, N. N. Chen, Y. Zhang, Y. W. Ma, X. F. Liu, Q. L. Fan, L. H. Wang, W. Huang, *J. Mater. Chem. A.*, 1 (2013) 12818.
19. H. Li, L. X. Jiang, Q. L. Cheng, Y. He, V. Pavlinek, P. Saha, C. Z. Li, *Electrochim. Acta*, 164 (2015) 252.
20. Z. Liu, C. L. Zhang, L. Luo, Z. Chang, X. M. Sun, *J. Mater. Chem.*, 22 (2012) 12149.
21. C. J. Xu, B. H. Li, H. D. Du, F. Y. Kang, Y. Q. Zeng, *J. Power Sources*, 184 (2008) 691.
22. X. L. Wang, X. Y. Fan, G. Li, M. Li, X. C. Xiao, A. P. Yu, Z. W. Chen, *Carbon*, 93 (2015) 258.
23. A. B. Chen, Y. F. Yu, T. T. Xing, R. J. Wang, Y. Zhang, Q. Li, *J. Mater. Sci.*, 50 (2015) 5578.
24. A. Singh, A. Chandra, *Sci. Rep.*, 5 (2015) 15551.
25. L. Huang, D. C. Chen, Y. Ding, S. Feng, Z. L. Wang, M. L. Liu, *Nano Lett.*, 13 (2013) 3135.
26. Y. X. Zhang, F. Li, M. Huang, *Mater. Lett.*, 112 (2013) 203.
27. D. Antiohos, K. Pingmuang, M. S. Romano, S. Beirne, T. Romeo, P. Aitchison, A. Minett, G. Wallace, S. Phanichphant, J. Chen, *Electrochim. Acta*, 101 (2013) 99.

© 2016 The Authors. Published by ESG ([www.electrochemsci.org](http://www.electrochemsci.org)). This article is an open access article distributed under the terms and conditions of the Creative Commons Attribution license (<http://creativecommons.org/licenses/by/4.0/>).